

Indoor Scene Reconstruction with Fine-Grained Details Using Hybrid Representation and Normal Prior Enhancement

Sheng Ye¹, Yubin Hu¹, Matthieu Lin¹, Yu-Hui Wen², Wang Zhao¹, Wenping Wang³,
Fellow, IEEE, Yong-Jin Liu¹, Senior Member, IEEE

¹Tsinghua University, ²Beijing Jiaotong University, ³Texas A&M University

Abstract

The reconstruction of indoor scenes from multi-view RGB images is challenging due to the coexistence of flat and texture-less regions alongside delicate and fine-grained regions. Recent methods leverage neural radiance fields aided by predicted surface normal priors to recover the scene geometry. These methods excel in producing complete and smooth results for floor and wall areas. However, they struggle to capture complex surfaces with high-frequency structures due to the inadequate neural representation and the inaccurately predicted normal priors. To improve the capacity of the implicit representation, we propose a hybrid architecture to represent low-frequency and high-frequency regions separately. To enhance the normal priors, we introduce a simple yet effective image sharpening and denoising technique, coupled with a network that estimates the pixel-wise uncertainty of the predicted surface normal vectors. Identifying such uncertainty can prevent our model from being misled by unreliable surface normal supervisions that hinder the accurate reconstruction of intricate geometries. Experiments on the benchmark datasets show that our method significantly outperforms existing methods in terms of reconstruction quality.

1 Introduction

3D reconstruction of a target scene from a sequence of multi-view RGB images is a fundamental problem in computer vision, which has a wide range of applications in various fields, including robotics, gaming, virtual reality, and so on. Specifically, high-fidelity reconstruction of indoor scenes is extremely challenging because indoor scenes have both large flat areas (floor, wall, roof) and high-frequency, fine-grained areas (small stuff on the table, delicate furniture).

Encoding scenes with the neural implicit function (Park et al. 2019; Mescheder et al. 2019; Sitzmann et al. 2020) has attracted increasing attention due to its compactness. Some recent works have achieved remarkable results in 3D scene reconstruction from 2D supervision by combining neural implicit function and differentiable volume rendering. NeuS (Wang et al. 2021) and VolSDF (Yariv et al. 2021) can reconstruct high-quality watertight surfaces of a single object by representing the geometry as an implicit signed distance field (SDF). Follow-up works try to integrate the im-

Copyright © 2024, Association for the Advancement of Artificial Intelligence (www.aaai.org). All rights reserved.

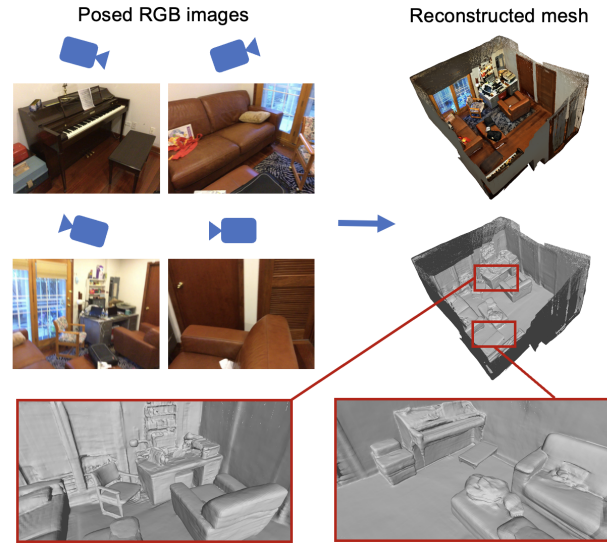


Figure 1: Our method can generate fine and accurate indoor scenes only from a sequence of posed RGB images.

PLICIT SDF representation and additional geometric priors, including semantic segmentation (Guo et al. 2022), monocular depth (Yu et al. 2022), or surface normals (Wang et al. 2022b), to address the challenge of indoor scene reconstruction. Compared to traditional MVS-based (Shen 2013; Schönberger et al. 2016) or TSDF-based (Murez et al. 2020; Stier et al. 2021) approaches, these neural implicit methods can produce complete and promising results, but still struggle with delicate and complex structures.

In this paper, we aim to reconstruct high-fidelity indoor scenes with fine and accurate details utilizing the implicit SDF framework (Wang et al. 2021). We first analyze two main limitations of the existing neural implicit methods that lead to the failure of fine-grained reconstruction. One of the limitations is that existing methods typically use a large MLP to approximate the implicit geometry function of the whole scene. Indeed, they can produce surprisingly good results for object-level surface reconstruction, but are less capable of recovering complicated indoor scenes. According to SIREN (Sitzmann et al. 2020) and MonoSDF (Yu et al. 2022), the deep MLP network possesses an inductive

smoothness bias and is therefore suitable to encode surfaces of flat and low-frequency areas. However, indoor scenes also consist of many high-frequency and fine-grained regions, which are difficult for a single MLP to express. Another limitation is that the surface normal priors used to regularize the implicit SDF may be inaccurate in regions with complex structures. These geometric priors are typically estimated by off-the-shelf neural networks (Bae, Budvytis, and Cipolla 2021; Eftekhari et al. 2021), which tend to produce noisy and erroneous results for thin and delicate structures. Models will be misled to generate wrong geometries when directly supervised by these inaccurate priors. Therefore, it is necessary to improve the quality of the predicted normal priors and design a mechanism to measure their reliability.

To improve the capacity of expressing both the flat areas and fine details, we design a novel hybrid representation. Specifically, we utilize an MLP network to encode the rough outline of the scene, and another branch of tri-plane features with a shallow decoder to represent the fine-grained details. To recover fine geometric details, some previous studies (Wang, Bleja, and Agapito 2022; Zhu et al. 2022; Wu et al. 2023) utilize the voxel grid features along with shallow MLP decoders. Nevertheless, they require complex training schemes and regularizations since the voxel representation tends to produce noisy surfaces. Moreover, the voxel grids are also memory-intensive due to their cubically growing consumption. Inspired by the remarkable performance of tri-plane representation in encoding human faces (Chan et al. 2022; Wang et al. 2023), we choose this memory-efficient representation instead of voxel grids to encode the delicate details. In our experiments, we empirically find that the tri-plane branch is suitable for expressing high-frequency details, which complements the MLP branch.

As for the enhancement of predicted normal priors, we observe that artifacts present in the input RGB images can greatly affect the quality of predicted normals. Thus, we apply a sharpening and denoising technique before feeding the images into the prior estimation module, which effectively reduces the errors in predicted normals. Furthermore, we design an uncertainty module, which predicts the pixel-wise uncertainty maps of the estimated normal priors. Besides the RGB images and monocular estimated normals, this module also takes features from the visual foundation model (Caron et al. 2021) as input to supplement the prediction with high-level semantic information. We then treat the predicted uncertainty as the weight of normal prior supervision. This uncertainty module reduces the negative impact of incorrectly predicted normal priors on reconstruction quality. In conclusion, we summarize our contributions as follows:

- We propose a hybrid implicit SDF architecture that incorporates MLP and tri-plane to better represent the low-frequency and high-frequency regions of indoor scenes.
- We design an image enhancement technique and an uncertainty estimation module to improve the quality of predicted geometric priors and guide our network to effectively leverage more accurate priors.
- Qualitative and quantitative experiments show that results generated by our method are significantly better

than the state-of-the-art methods. Apart from the commonly used datasets, our approach also generalizes well to real-world indoor scenarios captured by ourselves.

2 Related Works

2.1 Neural Surface Representation

Representing geometric surfaces by neural implicit functions has recently received increasing attention, because of its compactness and low memory consumption. The seminal work of DeepSDF (Park et al. 2019) first proposes to use a neural network to model a signed distance field, which encodes the underlying geometry of the target object. However, DeepSDF requires ground-truth 3D meshes to supervise the learning process. Recent methods incorporate neural implicit functions and differentiable rendering to reconstruct surfaces only from the supervision of multi-view images. IDR (Yariv et al. 2020) designs an architecture that simultaneously learns the implicit SDF field, camera poses, and a neural renderer. UNISURF (Oechsle, Peng, and Geiger 2021) utilizes occupancy to represent implicit surfaces and modifies the volume rendering equation correspondingly. Subsequently, NeuS (Wang et al. 2021) and VolSDF (Yariv et al. 2021) define the density used in volume rendering process as logistic sigmoid function and Laplace’s cumulative distribution function applied to an SDF representation. Nevertheless, all those works use a single MLP to approximate the implicit function, which struggles to scale to large and complicated scenes due to the network capacity. There also exist other researches (Peng et al. 2020; Zhu et al. 2022; Wang, Bleja, and Agapito 2022; Sun, Sun, and Chen 2022; Müller et al. 2022) that use multi-scale voxel grids followed by a shallow decoder to represent the scenes, but this leads to non-smoothness. We devise a novel hybrid representation incorporating MLP and tri-plane to enhance the network’s ability to express high-frequency and delicate surfaces.

2.2 Indoor Scene Reconstruction

Conventional multi-view stereo methods (Schönberger et al. 2016; Shen 2013) often struggle to reconstruct large textureless indoor scene areas densely. With the development of large-scale indoor datasets (Silberman et al. 2012; Xiao, Owens, and Torralba 2013; Dai et al. 2017), learning-based MVS methods are proposed to alleviate this problem. These methods (Yao et al. 2018, 2019; Im et al. 2019; Long et al. 2021; Sayed et al. 2022) typically predict a depth map for each frame and fuse these depth maps to build the final scene. However, the resulting surfaces tend to be noisy and incomplete due to the depth inconsistency problem. Another research branch (Murez et al. 2020; Sun et al. 2021; Stier et al. 2021; Yuan et al. 2023) proposes directly regressing input images to TSDF volume. Then the underlying mesh can be extracted from the TSDF volume using the marching-cube algorithm. Due to the limitation of TSDF volume resolution, the generated surfaces usually lack details.

Inspired by NeRF’s (Mildenhall et al. 2020) excellent performance in novel view synthesis tasks, some recent works attempt to leverage implicit surface representation and NeRF’s differentiable volume rendering to reconstruct

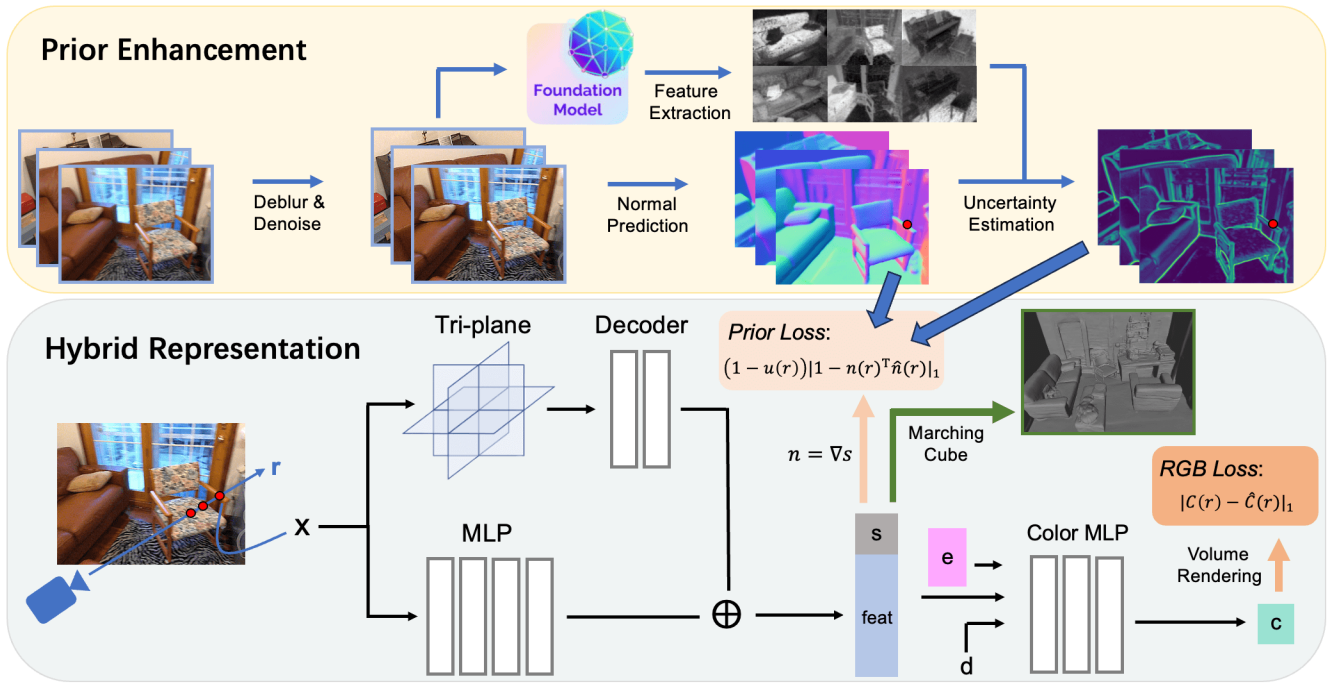


Figure 2: The overall pipeline of our proposed approach. We tackle high-frequency regions in scene reconstruction from the perspective of both the representation and geometric priors. In particular, we propose a hybrid representation to enhance the expressive power, and an image preprocessing technique along with pixel-wise uncertainty to enhance the normal priors.

indoor scenes. Considering the complexity of indoor scenes, additional priors are also provided to recover a plausible geometry. ManhattanSDF (Guo et al. 2022) utilizes extra 2D semantic segmentation to detect wall and floor regions, and applies geometry regularization based on Manhattan-world assumption. NeuRIS (Wang et al. 2022b) and MonoSDF (Yu et al. 2022) exploit monocular estimated normal and depth priors to reconstruct smooth surfaces. NeuRIS also devises a geometric checking technique to filter out unreasonable priors. HelixSurf (Liang et al. 2023) attempts to combine PatchMatch-based MVS and neural radiance fields, and proposes a joint optimization pipeline. Although these neural implicit methods significantly improve the reconstruction quality compared to conventional methods, surfaces in complex and fine-grained regions are still unsatisfactory. Furthermore, few studies have explored how to reduce the negative impact of inaccurate priors on reconstruction results.

2.3 Uncertainty Estimation

Uncertainty estimation, which aims to quantify the reliability of predictions, is crucial for many computer vision tasks such as optical flow (Ilg et al. 2018), SLAM (Kerl, Sturm, and Cremers 2013) and multi-view stereo (Wang et al. 2022a). Predicted uncertainty is used to facilitate the optimization through robust loss (Teed and Deng 2021), guided sampling (Sinha, Ebrahimi, and Darrell 2019), outlier rejection (Raguram, Frahm, and Pollefeys 2009), etc. However, the integration of the neural radiance field with uncertainty remains a relatively unexplored terrain. Some current efforts (Shen et al. 2021, 2022) mainly focus on the

task of rendering, while we focus on surface reconstruction. In this work, we novelly leverage the estimated uncertainty in a weighted loss to guide our model to utilize more precise priors while avoiding misguidance by less accurate ones.

3 Method

Our goal is to reconstruct high-fidelity, room-scale surfaces with fine and accurate details from multiple calibrated RGB images. We represent the scene geometry as an implicit SDF following the NeuS framework (Wang et al. 2021), and use surface normal maps estimated by an off-the-shelf network (Bae, Budvytis, and Cipolla 2021) to regularize our model. In the subsequent sections, we first briefly revisit the architecture of NeuS and its rendering equation. And then, we describe our proposed hybrid representation and normal prior enhancement techniques. Finally, we introduce the losses that are used to optimize our model. Figure 2 summarizes the overall pipeline of our proposed method.

3.1 Preliminary

The NeuS framework (Wang et al. 2021) mainly consists of two MLP networks: a geometry network f_g that outputs the SDF value s of any specified location \mathbf{x} , and a color network f_c that outputs the view-dependent emitted radiance c

$$s = f_g(\mathbf{x}; \theta_g), \quad c = f_c(\mathbf{x}, \mathbf{d}; \theta_c). \quad (1)$$

To reconstruct 3D scenes only from 2D supervision, NeuS adopts differentiable volume rendering. We denote a ray emitted from the camera as $\mathbf{r}(t) = \mathbf{o} + t\mathbf{d}$, where \mathbf{o} is

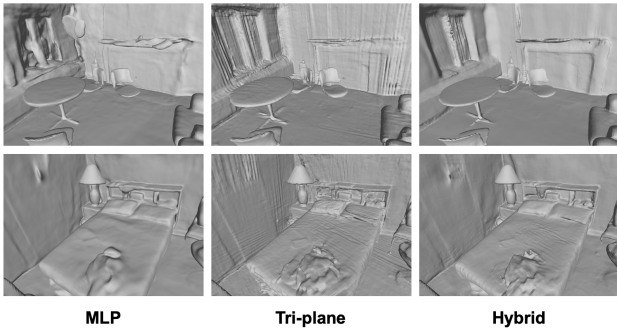


Figure 3: Comparison of the reconstructed meshes generated by different neural representations.

the camera center and \mathbf{d} is the viewing direction of the ray. Given a set of N sample points along the ray, the corresponding pixel color can be calculated as

$$C(\mathbf{r}) = \sum_{i=1}^N T_i \alpha_i \mathbf{c}(\mathbf{r}(t_i), \mathbf{d}), \quad T_i = \prod_{j=1}^{i-1} (1 - \alpha_j), \quad (2)$$

where α_i denotes the discrete opacity. According to NeuS, the opacity α_i is defined as

$$\alpha_i = \max \left(0, \frac{\Phi_\tau(f_g(\mathbf{r}(t_i))) - \Phi_\tau(f_g(\mathbf{r}(t_{i+1})))}{\Phi_\tau(f_g(\mathbf{r}(t_i)))} \right), \quad (3)$$

and Φ_τ is the Sigmoid function with a learnable parameter τ . After optimization of the model, the surface can then be extracted as the zero level-set of the SDF.

3.2 Hybrid Representation for Geometry

NeuS (Wang et al. 2021) utilizes a single MLP to represent the geometry of the entire indoor scene. Although equipped with positional encodings that encompass high-frequency bands, NeuS still tends to produce low-frequency surfaces and struggles to reconstruct complex and delicate structures. Recent researches (Sitzmann et al. 2020; Yu et al. 2022) have pointed out that the reasons may lie in the smoothness bias of MLP networks. MonoSDF (Yu et al. 2022) tries to replace the MLP with voxel grid features to recover fine details. However, the voxel representation is prone to generate noisy surfaces in the reconstruction results. Thus, it is highly desired to design a suitable architecture that can express both low-frequency and high-frequency structures.

Inspired by the success of EG3D (Chan et al. 2022), we use tri-planes to express the high-frequency features of indoor scenes. Besides being good at encoding detailed features, tri-planes are also memory-efficient, as their memory consumption only grows quadratically with the resolution. As shown in Figure 3, our preliminary experiments indicate the potential of using the tri-plane for scene reconstruction. The reconstructed 3D meshes of the tri-plane representation are sharper and possess more details than those generated by MLP representation. However, we also observe that using the tri-plane representation alone can cause striped artifacts in flat regions, such as walls and floors.

In order to accurately reconstruct both the flat areas and the fine-grained details, we propose a hybrid representation which contains an MLP branch and a tri-plane branch (see Figure 2). We aim to exploit the smoothness bias of MLP to encode the rough outline of the scene and the high-frequency bias of tri-plane features to encode the delicate structures. Given a 3D position $\mathbf{x} \in \mathbb{R}^3$, our pipeline first passes it through the MLP branch to get a coarse SDF value \tilde{s} and a coarse hidden feature $\tilde{\mathbf{h}}$. Then, the tri-plane branch refines these coarse outputs. Our tri-plane representation T consists of three axis-aligned orthogonal feature planes. Each feature plane has the dimension of $N \times N \times C$, where N is the spatial resolution, and C is the number of channels. We retrieve the final feature $[T_{xy}, T_{xz}, T_{yz}]$ by projecting \mathbf{x} onto these planes to find the tri-plane features and concatenating them together. A shallow, two-layer decoder further regresses the aggregated feature $[T_{xy}, T_{xz}, T_{yz}]$ to the residual SDF Δs and residual hidden feature $\Delta \mathbf{h}$. The final outputs are the summation of these two branches

$$\mathbf{s} = \tilde{s} + \Delta s, \quad \mathbf{h} = \tilde{\mathbf{h}} + \Delta \mathbf{h}. \quad (4)$$

Subsequently, we feed the hidden feature \mathbf{h} and the viewing direction \mathbf{d} into the color network to obtain the emitted radiance \mathbf{c} . Inspired by NeRF-W (Martin-Brualla et al. 2021), we also attach a learnable appearance embedding \mathbf{e} for each view as an extra input to the color network. Appearance embeddings aim to compensate for photometric and environmental variations between images and guarantee a multi-view consistent reconstruction. Our experiments demonstrate that cleaner and sharper surfaces can be obtained by using appearance embeddings.

We optimize the MLP and tri-plane branches simultaneously during the training process. To encourage them to focus on different areas of the scene, we initialize the MLP branch to produce an approximate SDF of a bounding sphere and the tri-plane branch to produce a zero SDF. As shown in Figure 3, our hybrid architecture combines the advantages of both representations and eliminates the striped artifacts as well. To the best of our knowledge, we are the first to utilize the tri-plane representation to compensate for high-frequency features in indoor scene reconstruction.

3.3 Prior Enhancement

Image Sharpening and Denoising Techniques. As indicated by NeuRIS (Wang et al. 2022b), normal priors predicted from off-the-shelf neural networks can serve as globally consistent geometric constraints, which lead to improved reconstruction quality. We also use the predicted normal priors as extra supervision. Specifically, we can obtain the surface normal under certain viewpoints using a similar volume accumulation process as Equation (2)

$$\mathbf{n}(\mathbf{r}) = \sum_{i=1}^N T_i \alpha_i \nabla \mathbf{s}_i, \quad (5)$$

where $\nabla \mathbf{s}_i$ is the gradient of SDF at sample points. During training, we minimize the difference between the normal calculated by our model and the pseudo ground-truth normal estimated by SNU (Bae, Budvytis, and Cipolla 2021).

It is worth noting that the estimated normal priors are not always accurate. We observe that artifacts of the input RGB images, especially noise and motion blur, can significantly affect the quality of estimated normal priors. Thus, we propose to use a sharpening and denoising enhancement before predicting the normal maps. For the sharpening process, we use a 3×3 kernel to perform convolution on the whole image. This kernel can be regarded as an edge detector, which amplifies the difference between the center pixel and its surrounding pixels. Formally, this operation is defined as

$$p'_i = 9 \cdot p_i - \sum_{p_j \in \mathcal{N}_i} p_j, \quad (6)$$

where p_i is the center pixel and \mathcal{N}_i is the eight neighboring pixels of p_i inside the 3×3 kernel. The sharpening process alleviates motion blur and strengthens edges in the images, facilitating the subsequent normal estimation of thin structures. For the denoising process, we employ the median filtering technique that replaces an image pixel with the median value of its neighbors. This operation can effectively remove the isolated noise while maintaining the sharpness of the image. We find that error-prone regions of the estimated normal priors are reduced after applying the denoising operation (more details can be found in our experiments).

Uncertainty Estimation Module. Our sharpening and denoising techniques can reduce the normal estimation errors caused by imperfect image quality. However, normal maps of complex and delicate regions are still hard to correctly estimate, even with high-quality input images. If directly supervised by normal priors without considering reliability, the model tends to ignore intricate structures and generate over-smooth geometries. Therefore, we design to attach a corresponding uncertainty map for each estimated normal map.

To predict the pixel-wise uncertainty of the estimated normal maps, we design a novel module as shown in Figure 4. This module adopts a U-Net (Ronneberger, Fischer, and Brox 2015) architecture with RGB images and the estimated normal maps as input. To supplement the uncertainty prediction with semantic information, we also input the high-level DINO (Caron et al. 2021) features into the module, since the normal uncertainty is usually semantic-relevant (low in flat and smooth regions, high in fine-grained regions). The semantic features are extracted from the last attention layer of the visual foundation model DINO. We train this uncertainty module on a subset (disjoint from the test set) of the ScanNet dataset (Dai et al. 2017). Concretely, we compute the difference between the estimated normals and normals rendered from real 3D meshes to obtain the ground-truth uncertainty maps, and use them to supervise our proposed module.

The pretrained uncertainty estimation module indicates the reliability of different regions of the estimated normal priors. Accordingly, we propose a weighted loss function when using these normal priors for supervision, which assigns larger (smaller) weights to the low (high) uncertainty areas. For the uncertainty value corresponding to a ray \mathbf{r} , we normalize it to $[0, 1]$, denoted as $\mathbf{u}(\mathbf{r})$. Then, our proposed

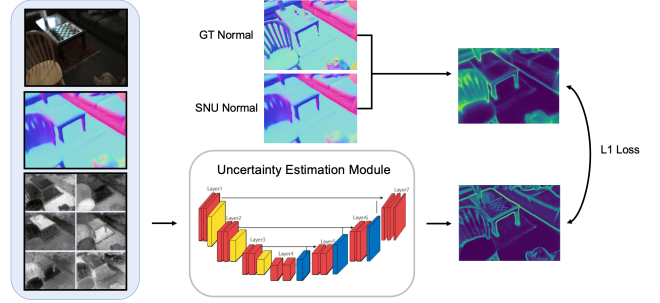


Figure 4: We propose an uncertainty estimation module to predict the pixel-wise uncertainty of the normal prior.

weighted loss function can be written as

$$\mathcal{L}_{prior} = \frac{1}{|\mathcal{R}|} \sum_{\mathbf{r} \in \mathcal{R}} (1 - \mathbf{u}(\mathbf{r})) \|1 - \mathbf{n}(\mathbf{r})^\top \hat{\mathbf{n}}(\mathbf{r})\|_1, \quad (7)$$

where \mathcal{R} is the set of rays in each batch, $\mathbf{n}(\mathbf{r})$ and $\hat{\mathbf{n}}(\mathbf{r})$ are the rendered normal and the pseudo ground-truth normal, respectively. In this way, our model can resist being misled by unreliable normal priors that hinder the accurate reconstruction of intricate and complex structures.

3.4 Loss Functions

The overall loss function is defined as

$$\mathcal{L} = \lambda_p \mathcal{L}_{prior} + \lambda_r \mathcal{L}_{rgb} + \lambda_e \mathcal{L}_{eik}. \quad (8)$$

The Eikonal loss \mathcal{L}_{eik} (Gropp et al. 2020) is used to constrain the gradient of SDF to be close to 1, which satisfies the Eikonal equation. And the RGB loss \mathcal{L}_{rgb} is defined as

$$\mathcal{L}_{rgb} = \frac{1}{|\mathcal{R}|} \sum_{\mathbf{r} \in \mathcal{R}} \|C(\mathbf{r}) - \hat{C}(\mathbf{r})\|_1, \quad (9)$$

where $C(\mathbf{r})$ and $\hat{C}(\mathbf{r})$ are the predicted and ground-truth RGB colors for ray \mathbf{r} respectively.

4 Experiments

4.1 Experiment Details

Datasets. We mainly conduct our experiments on ScanNet (Dai et al. 2017), and also demonstrate the generalization ability of our method on real-world scenes captured by ourselves. ScanNet is an indoor dataset containing 1,613 scenes with high-quality camera poses and 3D meshes. We use the same test split from ManhattanSDF (Guo et al. 2022).

Compared Methods. We compare our method with the following baselines: (1) Traditional MVS method COLMAP (Schönberger et al. 2016); (2) Data-driven methods, including SimpleRecon (Sayed et al. 2022), VoRTX (Stier et al. 2021), and 3D-Former (Yuan et al. 2023); (3) Neural implicit methods, including NeuS (Wang et al. 2021), ManhattanSDF (Guo et al. 2022), NeuRIS (Wang et al. 2022b), MonoSDF (MLP version and voxel grid version) (Yu et al. 2022), and HelixSurf (Liang et al. 2023).

Evaluation Metrics. Following previous methods, we use five standard metrics to evaluate the geometry quality: *Accuracy*, *Completeness*, *Precision*, *Recall*, and *F-score*. Refer to the supplementary material for their detailed definitions.

Implementation. Our proposed model is experimented on an NVIDIA A100 GPU. For the MLP branch, we adopt an 8-layer network; For the tri-plane, we adopt $256 \times 256 \times 16$ dimension. The uncertainty estimation module consists of 4 downsample convolution blocks and 4 upsample blocks. We implement our model in Pytorch using Adam optimizer. The loss weights are set to $\lambda_p = \lambda_r = 1.0$, $\lambda_e = 0.1$. In each batch, $|\mathcal{R}| = 512$. The training process takes 40k-50k iterations, depending on the scene’s complexity.

Table 1: Quantitative comparison of reconstruction quality on ScanNet dataset. Bold indicates the best.

Methods	Acc↓	Comp↓	Prec↑	Recall↑	F-score↑
COLMAP	0.047	0.235	0.711	0.441	0.537
SimpleRecon	0.058	0.045	0.677	0.755	0.713
VoRTX	0.052	0.063	0.713	0.630	0.668
3D-Former	0.035	0.048	0.803	0.708	0.752
NeuS	0.179	0.208	0.313	0.275	0.291
ManhattanSDF	0.072	0.068	0.621	0.586	0.602
NeuRIS	0.051	0.048	0.720	0.674	0.696
MonoSDF (Grid)	0.072	0.057	0.660	0.601	0.626
MonoSDF (MLP)	0.035	0.048	0.799	0.681	0.733
HelixSurf	0.038	0.044	0.786	0.727	0.755
Ours	0.033	0.041	0.814	0.737	0.773

4.2 Comparisons

Quantitative Evaluation. Table 1 summarizes quantitative comparison results on the ScanNet dataset. We compare our method with state of the arts and report the averaged metrics over all the test scenes. Note that our proposed method surpasses existing methods on all five metrics. F-score is usually regarded as a faithful metric for evaluating geometry quality as it considers both accuracy and completeness. In particular, we achieve remarkable improvement on F-score, which indicates that our approach can produce high-quality reconstructed meshes with fine and accurate details.

Qualitative Evaluation. We visualize the meshes reconstructed by different methods in Figure 5. SimpleRecon (Sayed et al. 2022) estimates and fuses per-frame depth maps, often leading to incomplete and noisy surfaces due to the problem of depth inconsistency. Results generated by 3D-Former (Yuan et al. 2023) are visually rough and lack details, as 3D-Former directly regresses the input images to TSDF volume. NeuRIS (Wang et al. 2022b) and MonoSDF (MLP version) (Yu et al. 2022) adopt large MLPs to encode the scene aided by geometric priors. Due to the limited expression capacity of MLP, NeuRIS tends to produce artifacts in complex and intricate regions. Similarly, MonoSDF cannot faithfully reconstruct thin and fine-grained structures, which is also demonstrated by low recall metrics in Table

Table 2: Ablation study of each component of our approach.

Config	Acc↓	Comp↓	Prec↑	Recall↑	F-score↑
MLP only	0.036	0.045	0.783	0.703	0.739
Tri-plane only	0.038	0.042	0.782	0.722	0.750
MLP + Grid	0.040	0.047	0.783	0.711	0.745
w/o embed	0.035	0.043	0.798	0.721	0.757
w/o enhance	0.043	0.045	0.774	0.719	0.745
w/o uncertainty	0.034	0.042	0.808	0.728	0.766
full model	0.033	0.041	0.814	0.737	0.773

1. HelixSurf (Liang et al. 2023) leverages MVS predictions to obtain a more complete geometry. However, as shown in Figure 5, HelixSurf generates inaccurate results in corner and edge areas. Compared with baselines, our method is visually appealing with clean and delicate surfaces. We show more qualitative results on real-world scenarios captured by ourselves and other datasets in supplementary material.

4.3 Ablation Study

We conduct ablation experiments by separately changing or removing one of these components: (a) the hybrid geometry representation; (b) the appearance embeddings (w/o embed); (c) the prior enhancement (w/o enhance); (d) the uncertainty estimation module (w/o uncertainty). Table 2 shows the results of our ablation study.

Analysis of Hybrid Representation. Experimental results show that replacing the hybrid representation with a single representation (MLP only / Tri-plane only) leads to a drastic drop in performance, suggesting that both MLP and tri-plane are necessary and complementary to each other. We have also tried to combine MLP with the voxel grid to enhance expressivity, but the performance of using voxel grid (MLP + Grid) is worse than using tri-plane (full model).

Analysis of Appearance Embedding. Since we only supervise our model on 2D observations, the inconsistency caused by photometric and environmental variations can lead to noisy geometries. Our experiments illustrate that the appearance embedding can alleviate this problem. We render the RGB images, normal maps, and depth maps in Figure 6. Note that the rendered depth maps and normal maps are sharper and cleaner by adding appearance embeddings.

Analysis of Prior Enhancement. As illustrated in Figure 6, motion blur during the video capture can cause wrong predictions of normal priors (e.g., bottom of the piano), which hinders the reconstruction of fine and accurate geometries. After applying our proposed enhancement technique, the input image becomes sharper, and the predicted normal map gets better. As a result, the accuracy and completeness of reconstructed meshes are improved as well.

Analysis of Uncertainty Estimation. By exploiting the estimated uncertainty as a measure of reliability, our model can be guided to focus on accurate normal priors. Ablation results show that the uncertainty estimation module helps to improve geometry quality. We visualize the reconstructed meshes and rendered normal maps in Figure 7. Adding un-

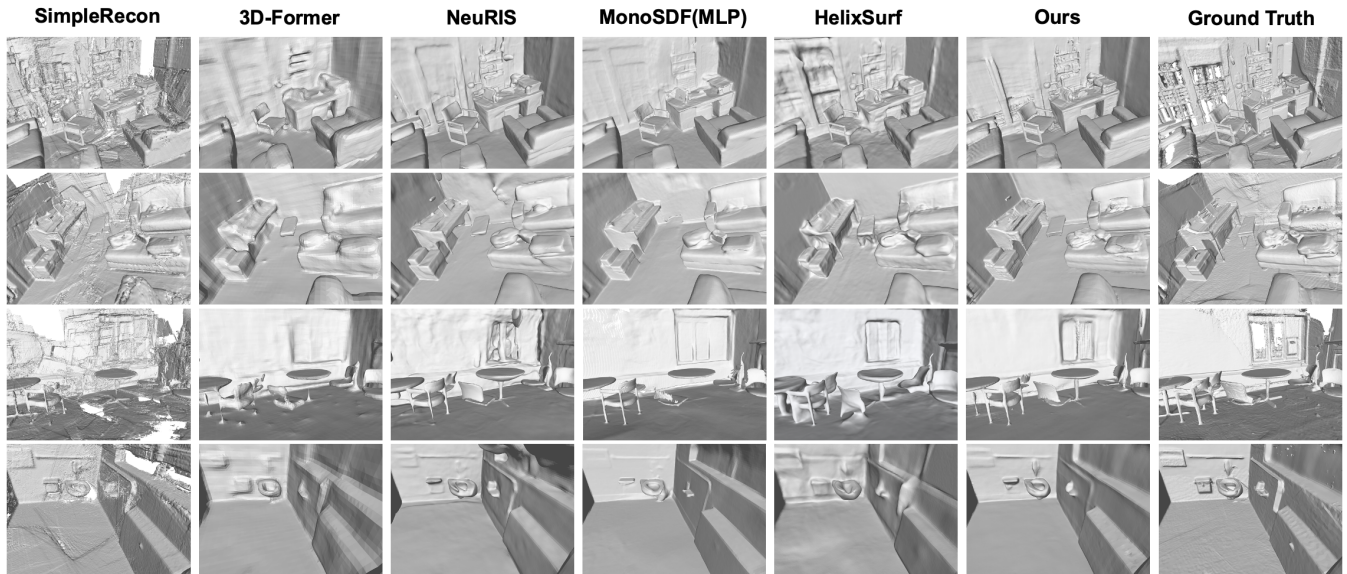


Figure 5: Qualitative comparison of our method with baselines on ScanNet dataset.

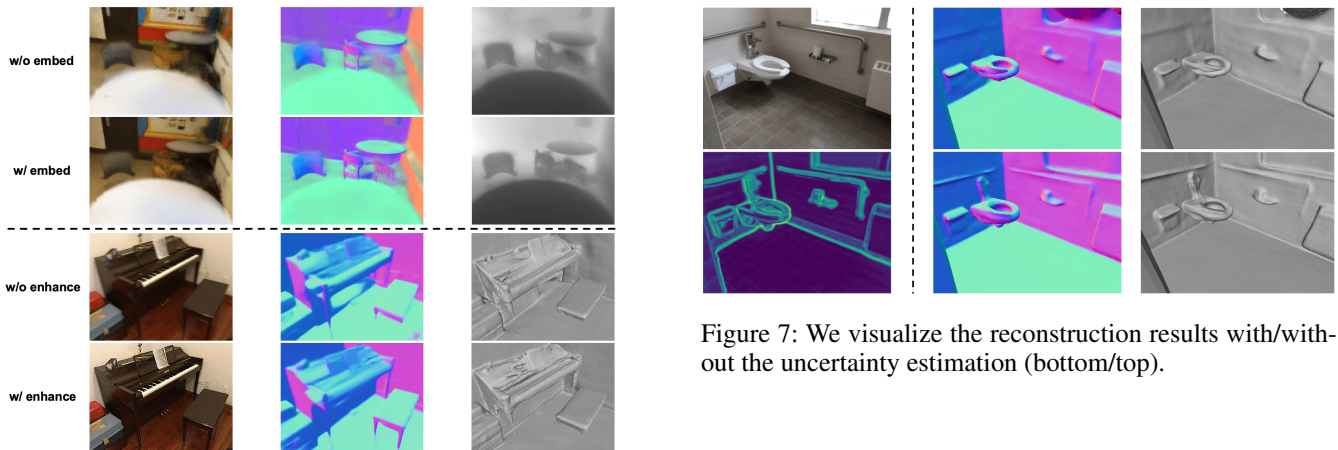


Figure 7: We visualize the reconstruction results with/without the uncertainty estimation (bottom/top).

Figure 6: We visualize the effects of appearance embeddings (top) and prior enhancement (bottom).

certainty as guidance makes the reconstruction results more visually appealing and richer in high-frequency details, especially in regions of complicated and delicate structures.

4.4 Real World Scenarios

In order to evaluate the generalization and practicality of our method, we also conduct experiments on real-world indoor scenarios captured by ourselves. Specifically, we walk around the scene and capture a video with our hand-held mobile phone. We extract 400-500 frames from this video and utilize OpenMVG (Moulon et al. 2016) to estimate camera poses. Figure 8 shows that our approach can produce high-fidelity meshes under different types of indoor scenes.

5 Conclusion

This paper proposes a novel framework to reconstruct indoor scenes with fine-grained details from a set of posed RGB images. To enhance the expressive capability of the network, we design a hybrid geometry representation to encode low-frequency and high-frequency structures separately. This hybrid representation incorporates the advantages of tri-plane and MLP. Besides, we propose a sharpening and denoising enhancement as well as an uncertainty estimation module. The enhancement technique can facilitate the prediction of sharper and clearer normal priors, and the estimated uncertainty maps can prevent our model from being misled by unreliable priors in intricate regions. Quantitative and qualitative experiments on ScanNet show that our approach significantly surpasses existing state-of-the-art methods. Furthermore, our model also generalizes well to real-world scenarios captured by hand-held mobile phones. In the future, we aim to speed up the training process for real-time reconstruction and extend our method to very large scenes.

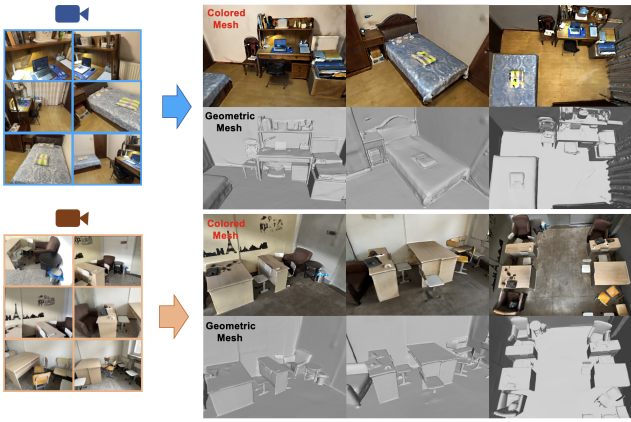


Figure 8: Our method generalizes well to real-world indoor scenarios captured by hand-held mobile phones.

6 Appendix

6.1 Network Architecture

Our reconstruction model utilizes one branch to encode the geometry (signed distance field) and another to encode the color (radiance field). Figure 9 illustrates the overall architecture. The geometry branch adopts a hybrid representation consisting of an eight-layer MLP and tri-plane features with a two-layer decoder. The final outputs of the SDF value and hidden feature are the MLP and tri-plane modules’ summation. The color branch takes the hidden feature, normal vector, position, viewing direction, and appearance embedding as inputs and adopts a four-layer MLP. Following NeRF (Mildenhall et al. 2020), we also apply positional encoding $\gamma(\cdot)$ to the input position x and viewing direction d .

Our uncertainty estimation model leverages a U-Net architecture (Ronneberger, Fischer, and Brox 2015) with skip connections. Specifically, the model contains four downsample convolution blocks and four upsample blocks. We select 300 scenes (disjoint from the test set) from the ScanNet dataset (Dai et al. 2017) and construct 12696 data pairs to train this network.

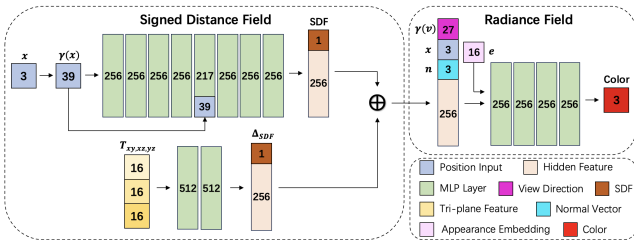


Figure 9: The overall architecture of our proposed model, consisting of a geometry branch and a color branch.

6.2 Analysis of Hybrid Representation

Our hybrid geometry representation contains an MLP module and a tri-plane module. To further analyze the effect of these two modules, we visualize the coarse mesh extracted

from the MLP branch and the fine mesh modulated by the tri-plane branch. Figure 10 demonstrates the results. The MLP branch can only output a rough outline of the scenes (floor, wall, etc.) without fine-grained details, while the tri-plane branch complement for smoother surfaces and delicate, high-frequency structures.

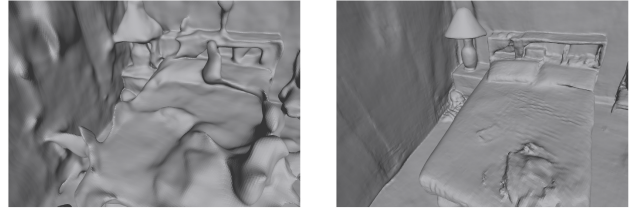


Figure 10: Coarse mesh (left) extracted from the MLP branch and fine mesh (right) modulated by the tri-plane branch.

6.3 Effects of DINO Features

We also use the high-level DINO (Caron et al. 2021) features as extra inputs when predicting uncertainty maps, since the normal uncertainty is usually semantic-relevant. Table 3 confirms that DINO features indeed help improve geometry.

Table 3: Effects of DINO features on reconstruction results

Config	Acc↓	Comp↓	Prec↑	Recall↑	F-score↑
w/o DINO	0.034	0.041	0.811	0.733	0.770
w/ DINO	0.033	0.041	0.814	0.737	0.773

6.4 Novel View Synthesis

The novel view is another form of understanding 3D scenes apart from meshes. In this work, our primary goal is to reconstruct high-fidelity, detailed surfaces of an indoor scenario. Facilitated by the accurate reconstruction results, we can also synthesize realistic images under novel views. As we select one image as input every ten frames to train our model, we use the remaining nine views to conduct rendering. Figure 11 shows the rendering results of our approach.

6.5 Additional Comparison Results

Evaluation Metrics. To evaluate the 3D reconstruction quality, we use five standard metrics described in Atlas (Murez et al. 2020): *Accuracy*, *Completeness*, *Precision*, *Recall*, and *F-score*. These metrics are defined in Table 4, where P and P^* denote the sample points from the predicted and ground-truth mesh.

6.6 Visualization of Normal Maps

To further compare the reconstruction results of our method and other existing baselines, we visualize the normal maps rendered from the reconstructed meshes. Figure 13 and Figure 14 demonstrate the qualitative comparison results. Note

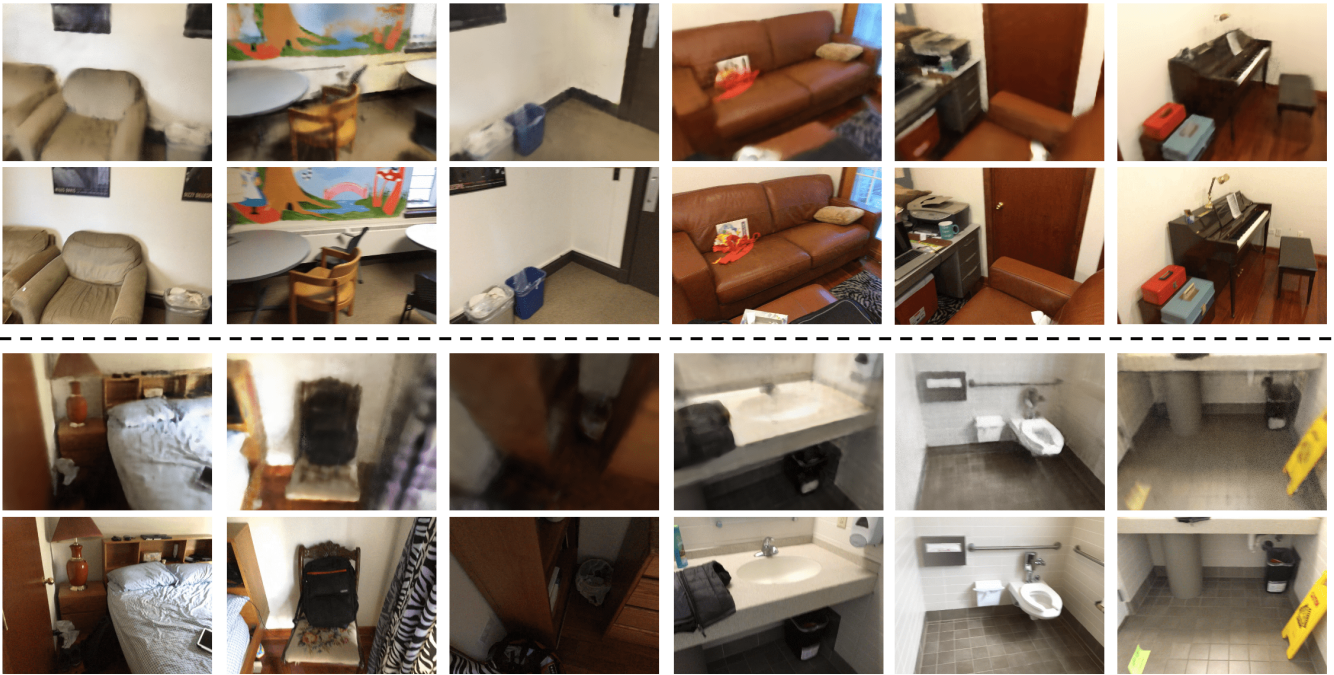


Figure 11: Results of the novel view synthesis task. In each block, the first row is our rendering results, and the second row is the corresponding ground-truth images.

Table 4: Definitions of the metrics to evaluate the 3D reconstruction quality.

3D Metric	Definition
<i>Accuracy</i>	$\text{mean}_{p \in P}(\min_{p^* \in P^*} \ p - p^*\)$
<i>Completeness</i>	$\text{mean}_{p^* \in P^*}(\min_{p \in P} \ p - p^*\)$
<i>Precision</i>	$\text{mean}_{p \in P}(\min_{p^* \in P^*} \ p - p^*\ < 0.05)$
<i>Recall</i>	$\text{mean}_{p^* \in P^*}(\min_{p \in P} \ p - p^*\ < 0.05)$
<i>F-Score</i>	$\frac{2 \times \text{Precision} \times \text{Recall}}{\text{Precision} + \text{Recall}}$

that our approach can generate visually appealing geometry with fine details, which surpasses other state-of-the-art methods.

6.7 Generalization Ability

Our quantitative experiments on the ScanNet dataset (Dai et al. 2017) demonstrate the remarkable performance of our method. In order to further examine the generalization ability of our model, we also test on Replica dataset (Straub et al. 2019) and real-world scenes. Different from ScanNet, Replica is a human-generated synthetic dataset with high-quality rendering images and accurate camera poses. For the real-world scenario, we capture a video of two minutes with our mobile phone and extract several hundred frames to train the model. The corresponding camera poses are obtained by OpenMVG (Moulon et al. 2016). The reconstruction results are shown in Figure 15 and Figure 16, which indicate that our approach performs well on both synthetic and real data.

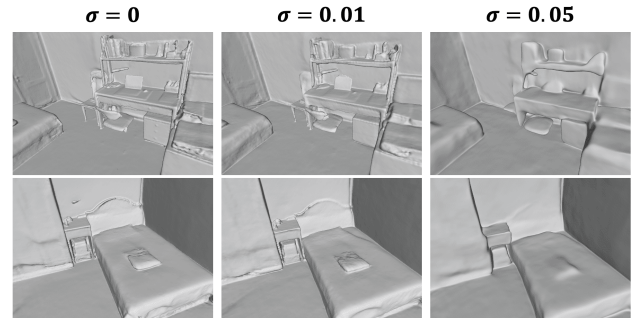


Figure 12: Reconstructed meshes under noisy camera poses (σ indicates the noise intensity). Note that our approach can still produce reasonable surfaces.

6.8 Robustness

In this work, we assume the camera poses in datasets are precise. However, the camera calibration process may introduce some errors under real circumstances. To evaluate the robustness of our method under extremely noisy poses, we add a random perturbation (between $[0, \sigma]$) to the camera pose of each view and conduct the 3D reconstruction. As illustrated in Figure 12, our method can still generate plausible geometry under noisy camera poses.

References

Bae, G.; Budvytis, I.; and Cipolla, R. 2021. Estimating and Exploiting the Aleatoric Uncertainty in Surface Normal Estimation. In *2021 IEEE/CVF International Conference on*

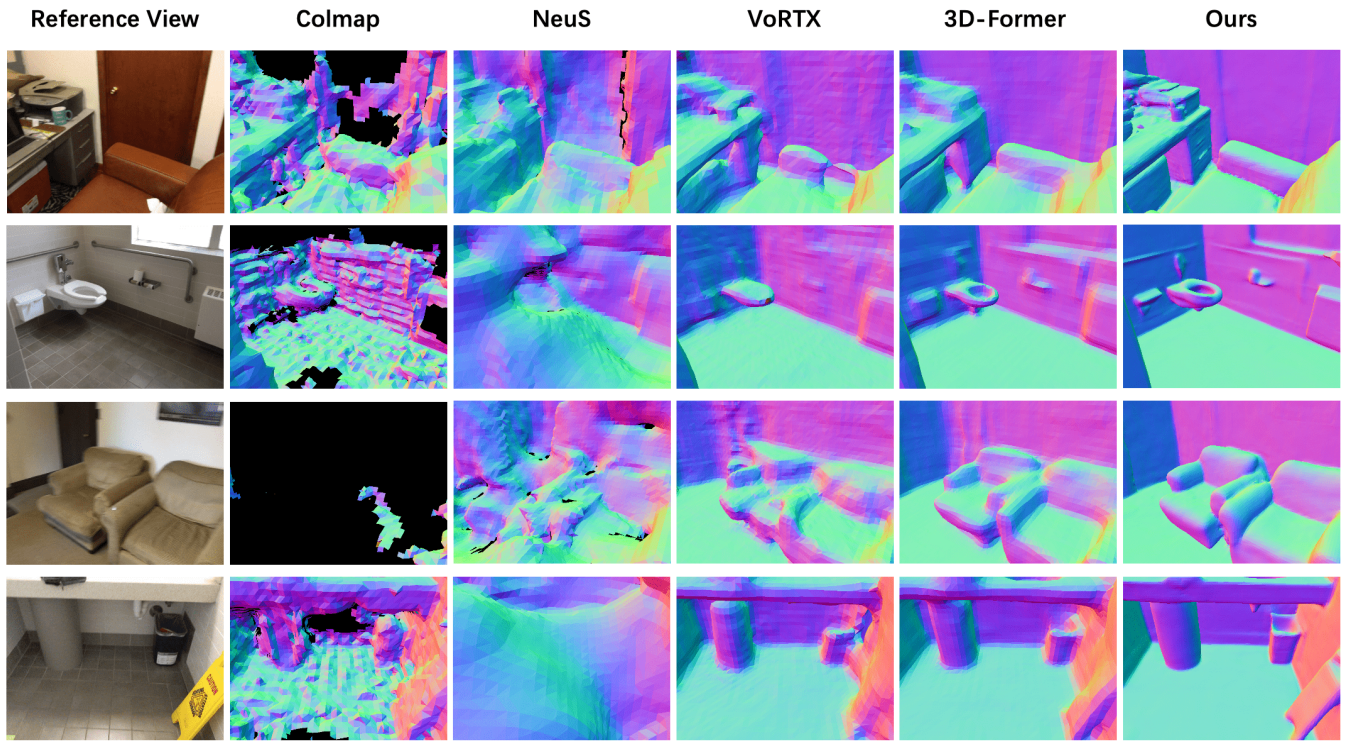


Figure 13: Qualitative comparison of normal maps (first part).

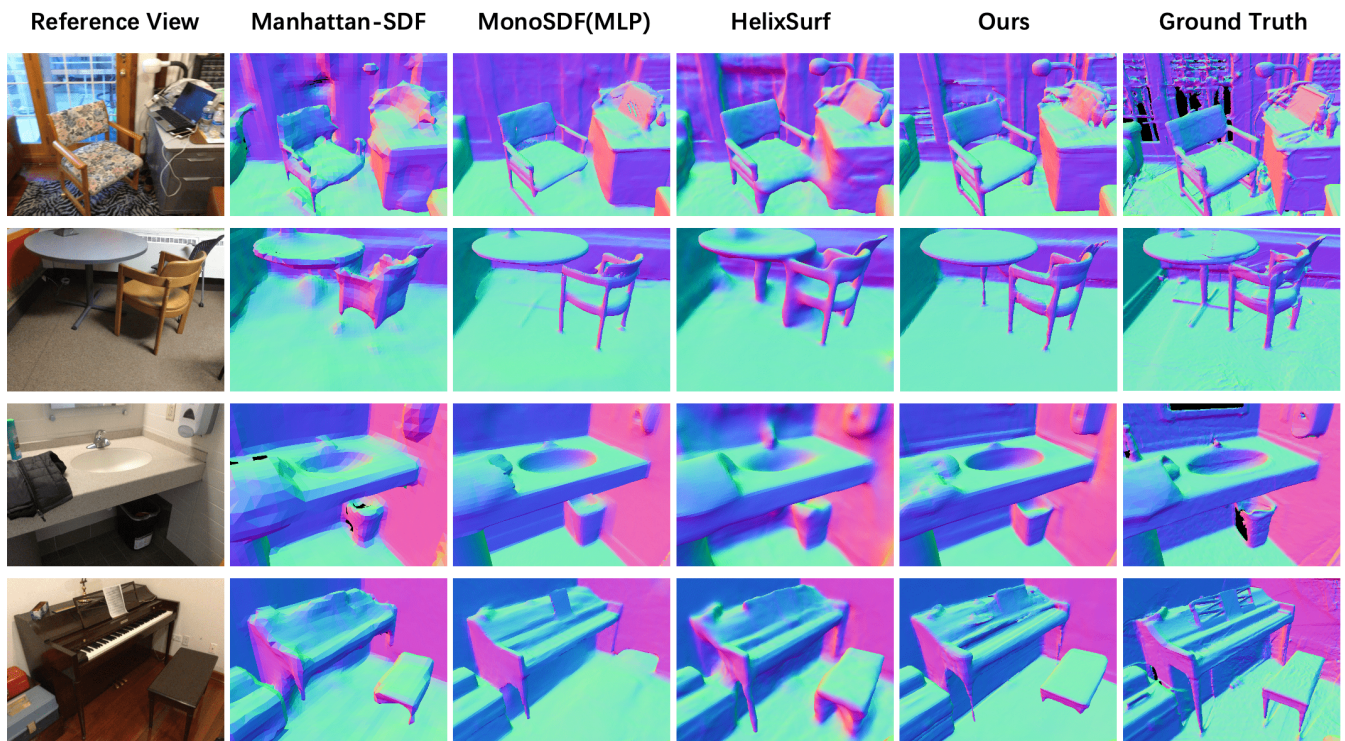


Figure 14: Qualitative comparison of normal maps (second part).

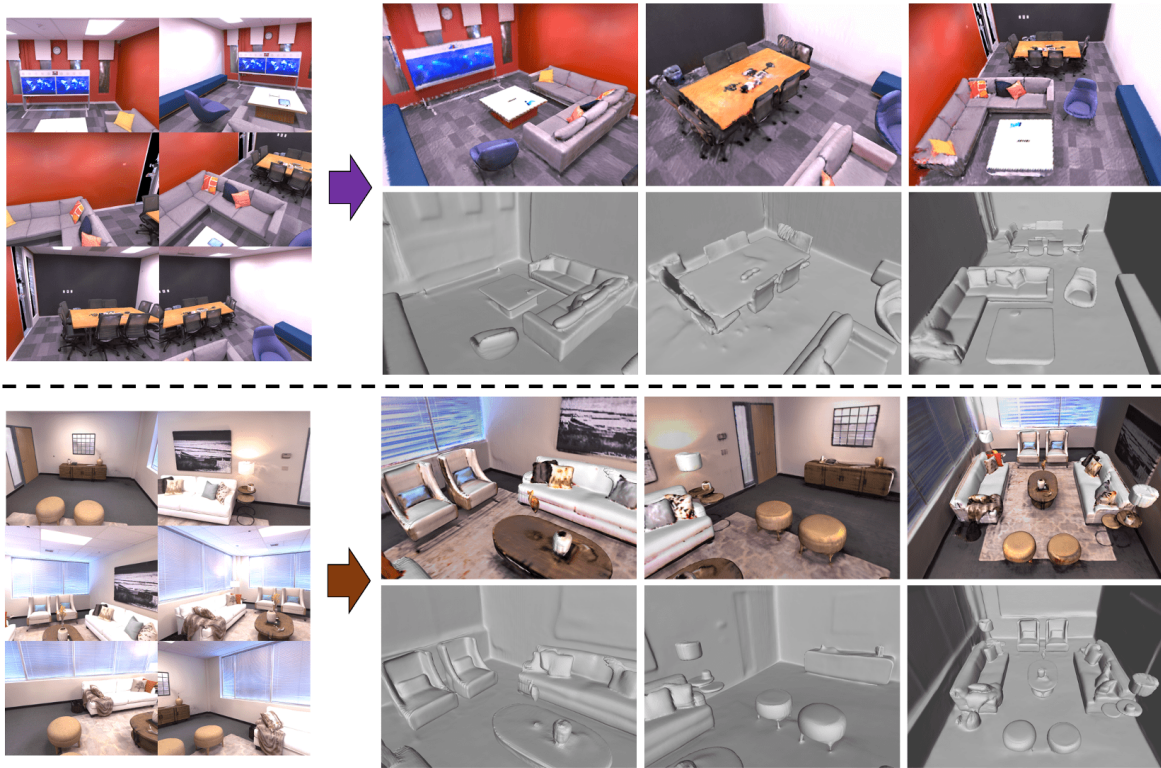


Figure 15: Reconstruction results on Replica dataset.

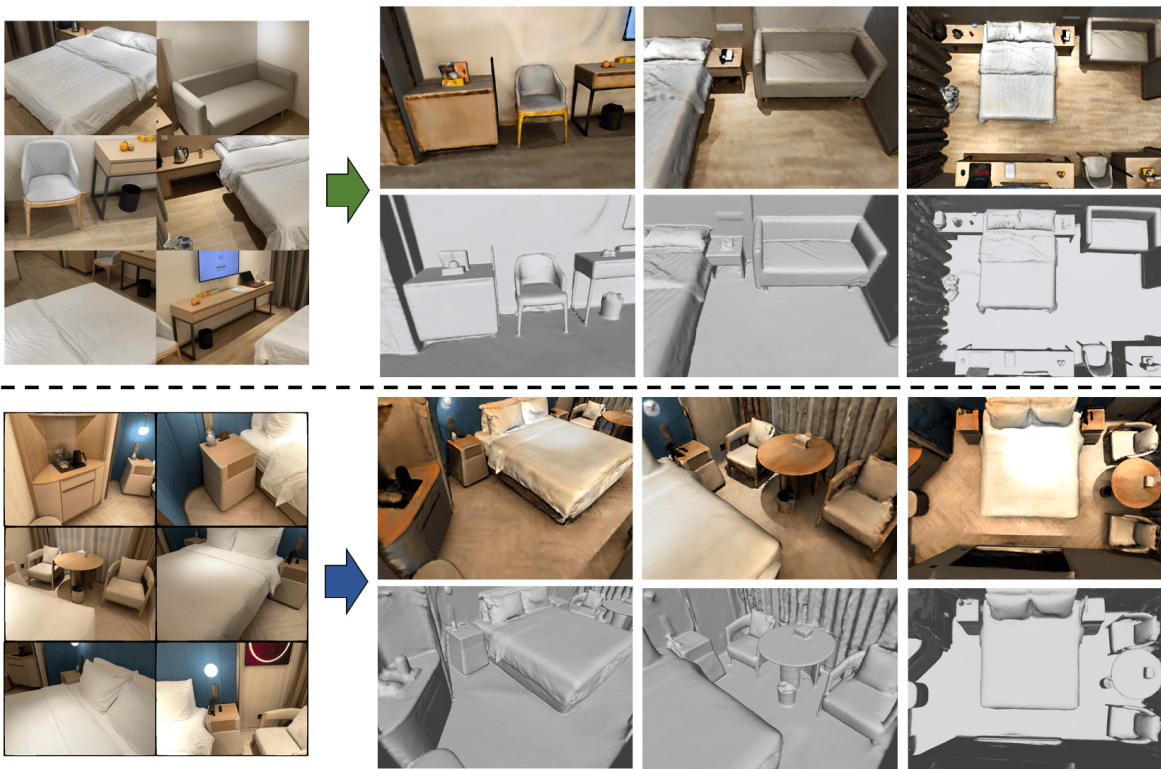


Figure 16: Reconstruction results on real-world indoor scenes.

- Computer Vision, ICCV 2021, Montreal, QC, Canada, October 10-17, 2021, 13117–13126. IEEE.
- Caron, M.; Touvron, H.; Misra, I.; Jégou, H.; Mairal, J.; Bojanowski, P.; and Joulin, A. 2021. Emerging Properties in Self-Supervised Vision Transformers. In *2021 IEEE/CVF International Conference on Computer Vision, ICCV 2021, Montreal, QC, Canada, October 10-17, 2021*, 9630–9640. IEEE.
- Chan, E. R.; Lin, C. Z.; Chan, M. A.; Nagano, K.; Pan, B.; Mello, S. D.; Gallo, O.; Guibas, L. J.; Tremblay, J.; Khamis, S.; Karras, T.; and Wetzstein, G. 2022. Efficient Geometry-aware 3D Generative Adversarial Networks. In *IEEE/CVF Conference on Computer Vision and Pattern Recognition, CVPR 2022, New Orleans, LA, USA, June 18-24, 2022*, 16102–16112. IEEE.
- Dai, A.; Chang, A. X.; Savva, M.; Halber, M.; Funkhouser, T. A.; and Nießner, M. 2017. ScanNet: Richly-Annotated 3D Reconstructions of Indoor Scenes. In *2017 IEEE Conference on Computer Vision and Pattern Recognition, CVPR 2017, Honolulu, HI, USA, July 21-26, 2017*, 2432–2443. IEEE Computer Society.
- Eftekhari, A.; Sax, A.; Malik, J.; and Zamir, A. 2021. Omnidata: A scalable pipeline for making multi-task mid-level vision datasets from 3d scans. In *Proceedings of the IEEE/CVF International Conference on Computer Vision*, 10786–10796.
- Gropp, A.; Yariv, L.; Haim, N.; Atzmon, M.; and Lipman, Y. 2020. Implicit Geometric Regularization for Learning Shapes. In *Proceedings of the 37th International Conference on Machine Learning, ICML 2020, 13-18 July 2020, Virtual Event*, volume 119 of *Proceedings of Machine Learning Research*, 3789–3799. PMLR.
- Guo, H.; Peng, S.; Lin, H.; Wang, Q.; Zhang, G.; Bao, H.; and Zhou, X. 2022. Neural 3D Scene Reconstruction with the Manhattan-world Assumption. In *IEEE/CVF Conference on Computer Vision and Pattern Recognition, CVPR 2022, New Orleans, LA, USA, June 18-24, 2022*, 5501–5510. IEEE.
- Ilg, E.; Cicek, O.; Galesso, S.; Klein, A.; Makansi, O.; Hutter, F.; and Brox, T. 2018. Uncertainty estimates and multi-hypotheses networks for optical flow. In *Proceedings of the European Conference on Computer Vision (ECCV)*, 652–667.
- Im, S.; Jeon, H.; Lin, S.; and Kweon, I. S. 2019. DPSNet: End-to-end Deep Plane Sweep Stereo. In *7th International Conference on Learning Representations, ICLR 2019, New Orleans, LA, USA, May 6-9, 2019*. OpenReview.net.
- Kerl, C.; Sturm, J.; and Cremers, D. 2013. Dense visual SLAM for RGB-D cameras. In *2013 IEEE/RSJ International Conference on Intelligent Robots and Systems*, 2100–2106. IEEE.
- Liang, Z.; Huang, Z.; Ding, C.; and Jia, K. 2023. HelixSurf: A Robust and Efficient Neural Implicit Surface Learning of Indoor Scenes with Iterative Intertwined Regularization. In *Proceedings of the IEEE/CVF Conference on Computer Vision and Pattern Recognition*, 13165–13174.
- Long, X.; Liu, L.; Li, W.; Theobalt, C.; and Wang, W. 2021. Multi-view Depth Estimation using Epipolar Spatio-Temporal Networks. In *IEEE Conference on Computer Vision and Pattern Recognition, CVPR 2021, virtual, June 19-25, 2021*, 8258–8267. Computer Vision Foundation / IEEE.
- Martin-Brualla, R.; Radwan, N.; Sajjadi, M. S. M.; Barron, J. T.; Dosovitskiy, A.; and Duckworth, D. 2021. NeRF in the Wild: Neural Radiance Fields for Unconstrained Photo Collections. In *IEEE Conference on Computer Vision and Pattern Recognition, CVPR 2021, virtual, June 19-25, 2021*, 7210–7219. Computer Vision Foundation / IEEE.
- Mescheder, L. M.; Oechsle, M.; Niemeyer, M.; Nowozin, S.; and Geiger, A. 2019. Occupancy Networks: Learning 3D Reconstruction in Function Space. In *IEEE Conference on Computer Vision and Pattern Recognition, CVPR 2019, Long Beach, CA, USA, June 16-20, 2019*, 4460–4470. Computer Vision Foundation / IEEE.
- Mildenhall, B.; Srinivasan, P. P.; Tancik, M.; Barron, J. T.; Ramamoorthi, R.; and Ng, R. 2020. NeRF: Representing Scenes as Neural Radiance Fields for View Synthesis. In Vedaldi, A.; Bischof, H.; Brox, T.; and Frahm, J., eds., *Computer Vision - ECCV 2020 - 16th European Conference, Glasgow, UK, August 23-28, 2020, Proceedings, Part I*, volume 12346 of *Lecture Notes in Computer Science*, 405–421. Springer.
- Moulon, P.; Monasse, P.; Perrot, R.; and Marlet, R. 2016. OpenMVG: Open Multiple View Geometry. In Kerautret, B.; Colom, M.; and Monasse, P., eds., *Reproducible Research in Pattern Recognition - First International Workshop, RRPR@ICPR 2016, Cancún, Mexico, December 4, 2016, Revised Selected Papers*, volume 10214 of *Lecture Notes in Computer Science*, 60–74.
- Müller, T.; Evans, A.; Schied, C.; and Keller, A. 2022. Instant neural graphics primitives with a multiresolution hash encoding. *ACM Trans. Graph.*, 41(4): 102:1–102:15.
- Murez, Z.; van As, T.; Bartolozzi, J.; Sinha, A.; Badrinarayanan, V.; and Rabinovich, A. 2020. Atlas: End-to-End 3D Scene Reconstruction from Posed Images. In Vedaldi, A.; Bischof, H.; Brox, T.; and Frahm, J., eds., *Computer Vision - ECCV 2020 - 16th European Conference, Glasgow, UK, August 23-28, 2020, Proceedings, Part VII*, volume 12352 of *Lecture Notes in Computer Science*, 414–431. Springer.
- Oechsle, M.; Peng, S.; and Geiger, A. 2021. UNISURF: Unifying Neural Implicit Surfaces and Radiance Fields for Multi-View Reconstruction. In *2021 IEEE/CVF International Conference on Computer Vision, ICCV 2021, Montreal, QC, Canada, October 10-17, 2021*, 5569–5579. IEEE.
- Park, J. J.; Florence, P. R.; Straub, J.; Newcombe, R. A.; and Lovegrove, S. 2019. DeepSDF: Learning Continuous Signed Distance Functions for Shape Representation. In *IEEE Conference on Computer Vision and Pattern Recognition, CVPR 2019, Long Beach, CA, USA, June 16-20, 2019*, 165–174. Computer Vision Foundation / IEEE.
- Peng, S.; Niemeyer, M.; Mescheder, L. M.; Pollefeys, M.; and Geiger, A. 2020. Convolutional Occupancy Networks. In Vedaldi, A.; Bischof, H.; Brox, T.; and Frahm, J., eds.,

- Computer Vision - ECCV 2020 - 16th European Conference, Glasgow, UK, August 23-28, 2020, Proceedings, Part III*, volume 12348 of *Lecture Notes in Computer Science*, 523–540. Springer.
- Raguram, R.; Frahm, J.-M.; and Pollefeys, M. 2009. Exploiting uncertainty in random sample consensus. In *2009 IEEE 12th International Conference on Computer Vision*, 2074–2081. IEEE.
- Ronneberger, O.; Fischer, P.; and Brox, T. 2015. U-net: Convolutional networks for biomedical image segmentation. In *Medical Image Computing and Computer-Assisted Intervention—MICCAI 2015: 18th International Conference, Munich, Germany, October 5-9, 2015, Proceedings, Part III 18*, 234–241. Springer.
- Sayed, M.; Gibson, J.; Watson, J.; Prisacariu, V.; Firman, M.; and Godard, C. 2022. SimpleRecon: 3D Reconstruction Without 3D Convolutions. In Avidan, S.; Brostow, G. J.; Cissé, M.; Farinella, G. M.; and Hassner, T., eds., *Computer Vision - ECCV 2022 - 17th European Conference, Tel Aviv, Israel, October 23-27, 2022, Proceedings, Part XXXIII*, volume 13693 of *Lecture Notes in Computer Science*, 1–19. Springer.
- Schönberger, J. L.; Zheng, E.; Frahm, J.; and Pollefeys, M. 2016. Pixelwise View Selection for Unstructured Multi-View Stereo. In Leibe, B.; Matas, J.; Sebe, N.; and Welling, M., eds., *Computer Vision - ECCV 2016 - 14th European Conference, Amsterdam, The Netherlands, October 11-14, 2016, Proceedings, Part III*, volume 9907 of *Lecture Notes in Computer Science*, 501–518. Springer.
- Shen, J.; Agudo, A.; Moreno-Noguer, F.; and Ruiz, A. 2022. Conditional-Flow NeRF: Accurate 3D Modelling with Reliable Uncertainty Quantification. In Avidan, S.; Brostow, G. J.; Cissé, M.; Farinella, G. M.; and Hassner, T., eds., *Computer Vision - ECCV 2022 - 17th European Conference, Tel Aviv, Israel, October 23-27, 2022, Proceedings, Part III*, volume 13663 of *Lecture Notes in Computer Science*, 540–557. Springer.
- Shen, J.; Ruiz, A.; Agudo, A.; and Moreno-Noguer, F. 2021. Stochastic Neural Radiance Fields: Quantifying Uncertainty in Implicit 3D Representations. In *International Conference on 3D Vision, 3DV 2021, London, United Kingdom, December 1-3, 2021*, 972–981. IEEE.
- Shen, S. 2013. Accurate Multiple View 3D Reconstruction Using Patch-Based Stereo for Large-Scale Scenes. *IEEE Trans. Image Process.*, 22(5): 1901–1914.
- Silberman, N.; Hoiem, D.; Kohli, P.; and Fergus, R. 2012. Indoor Segmentation and Support Inference from RGBD Images. In Fitzgibbon, A. W.; Lazebnik, S.; Perona, P.; Sato, Y.; and Schmid, C., eds., *Computer Vision - ECCV 2012 - 12th European Conference on Computer Vision, Florence, Italy, October 7-13, 2012, Proceedings, Part V*, volume 7576 of *Lecture Notes in Computer Science*, 746–760. Springer.
- Sinha, S.; Ebrahimi, S.; and Darrell, T. 2019. Variational adversarial active learning. In *Proceedings of the IEEE/CVF International Conference on Computer Vision*, 5972–5981.
- Sitzmann, V.; Martel, J. N. P.; Bergman, A. W.; Lindell, D. B.; and Wetzstein, G. 2020. Implicit Neural Representations with Periodic Activation Functions. In Larochelle, H.; Ranzato, M.; Hadsell, R.; Balcan, M.; and Lin, H., eds., *Advances in Neural Information Processing Systems 33: Annual Conference on Neural Information Processing Systems 2020, NeurIPS 2020, December 6-12, 2020, virtual*.
- Stier, N.; Rich, A.; Sen, P.; and Höllerer, T. 2021. VoRTX: Volumetric 3D Reconstruction With Transformers for Voxelwise View Selection and Fusion. In *International Conference on 3D Vision, 3DV 2021, London, United Kingdom, December 1-3, 2021*, 320–330. IEEE.
- Straub, J.; Whelan, T.; Ma, L.; Chen, Y.; Wijmans, E.; Green, S.; Engel, J. J.; Mur-Artal, R.; Ren, C.; Verma, S.; et al. 2019. The Replica dataset: A digital replica of indoor spaces. *arXiv preprint arXiv:1906.05797*.
- Sun, C.; Sun, M.; and Chen, H. 2022. Direct Voxel Grid Optimization: Super-fast Convergence for Radiance Fields Reconstruction. In *IEEE/CVF Conference on Computer Vision and Pattern Recognition, CVPR 2022, New Orleans, LA, USA, June 18-24, 2022*, 5449–5459. IEEE.
- Sun, J.; Xie, Y.; Chen, L.; Zhou, X.; and Bao, H. 2021. NeuralRecon: Real-Time Coherent 3D Reconstruction From Monocular Video. In *IEEE Conference on Computer Vision and Pattern Recognition, CVPR 2021, virtual, June 19-25, 2021*, 15598–15607. Computer Vision Foundation / IEEE.
- Teed, Z.; and Deng, J. 2021. Droid-slam: Deep visual slam for monocular, stereo, and rgb-d cameras. *Advances in neural information processing systems*, 34: 16558–16569.
- Wang, F.; Galliani, S.; Vogel, C.; and Pollefeys, M. 2022a. IterMVS: Iterative probability estimation for efficient multi-view stereo. In *Proceedings of the IEEE/CVF conference on computer vision and pattern recognition*, 8606–8615.
- Wang, J.; Bleja, T.; and Agapito, L. 2022. GO-Surf: Neural Feature Grid Optimization for Fast, High-Fidelity RGB-D Surface Reconstruction. In *International Conference on 3D Vision, 3DV 2022, Prague, Czech Republic, September 12-16, 2022*, 433–442. IEEE.
- Wang, J.; Wang, P.; Long, X.; Theobalt, C.; Komura, T.; Liu, L.; and Wang, W. 2022b. NeuRIS: Neural Reconstruction of Indoor Scenes Using Normal Priors. In Avidan, S.; Brostow, G. J.; Cissé, M.; Farinella, G. M.; and Hassner, T., eds., *Computer Vision - ECCV 2022 - 17th European Conference, Tel Aviv, Israel, October 23-27, 2022, Proceedings, Part XXXII*, volume 13692 of *Lecture Notes in Computer Science*, 139–155. Springer.
- Wang, P.; Liu, L.; Liu, Y.; Theobalt, C.; Komura, T.; and Wang, W. 2021. NeuS: Learning Neural Implicit Surfaces by Volume Rendering for Multi-view Reconstruction. In Ranzato, M.; Beygelzimer, A.; Dauphin, Y. N.; Liang, P.; and Vaughan, J. W., eds., *Advances in Neural Information Processing Systems 34: Annual Conference on Neural Information Processing Systems 2021, NeurIPS 2021, December 6-14, 2021, virtual*, 27171–27183.
- Wang, T.; Zhang, B.; Zhang, T.; Gu, S.; Bao, J.; Baltrusaitis, T.; Shen, J.; Chen, D.; Wen, F.; Chen, Q.; et al. 2023. Rodin: A generative model for sculpting 3d digital avatars using diffusion. In *Proceedings of the IEEE/CVF Conference on Computer Vision and Pattern Recognition*, 4563–4573.

Wu, T.; Wang, J.; Pan, X.; Xu, X.; Theobalt, C.; Liu, Z.; and Lin, D. 2023. Voxurf: Voxel-based Efficient and Accurate Neural Surface Reconstruction. In *The Eleventh International Conference on Learning Representations, ICLR 2023, Kigali, Rwanda, May 1-5, 2023*. OpenReview.net.

Xiao, J.; Owens, A.; and Torralba, A. 2013. SUN3D: A Database of Big Spaces Reconstructed Using SfM and Object Labels. In *IEEE International Conference on Computer Vision, ICCV 2013, Sydney, Australia, December 1-8, 2013*, 1625–1632. IEEE Computer Society.

Yao, Y.; Luo, Z.; Li, S.; Fang, T.; and Quan, L. 2018. MVS-Net: Depth Inference for Unstructured Multi-view Stereo. In Ferrari, V.; Hebert, M.; Sminchisescu, C.; and Weiss, Y., eds., *Computer Vision - ECCV 2018 - 15th European Conference, Munich, Germany, September 8-14, 2018, Proceedings, Part VIII*, volume 11212 of *Lecture Notes in Computer Science*, 785–801. Springer.

Yao, Y.; Luo, Z.; Li, S.; Shen, T.; Fang, T.; and Quan, L. 2019. Recurrent MVSNet for High-Resolution Multi-View Stereo Depth Inference. In *IEEE Conference on Computer Vision and Pattern Recognition, CVPR 2019, Long Beach, CA, USA, June 16-20, 2019*, 5525–5534. Computer Vision Foundation / IEEE.

Yariv, L.; Gu, J.; Kasten, Y.; and Lipman, Y. 2021. Volume Rendering of Neural Implicit Surfaces. In Ranzato, M.; Beygelzimer, A.; Dauphin, Y. N.; Liang, P.; and Vaughan, J. W., eds., *Advances in Neural Information Processing Systems 34: Annual Conference on Neural Information Processing Systems 2021, NeurIPS 2021, December 6-14, 2021, virtual*, 4805–4815.

Yariv, L.; Kasten, Y.; Moran, D.; Galun, M.; Atzmon, M.; Basri, R.; and Lipman, Y. 2020. Multiview Neural Surface Reconstruction by Disentangling Geometry and Appearance. In Larochelle, H.; Ranzato, M.; Hadsell, R.; Balcan, M.; and Lin, H., eds., *Advances in Neural Information Processing Systems 33: Annual Conference on Neural Information Processing Systems 2020, NeurIPS 2020, December 6-12, 2020, virtual*.

Yu, Z.; Peng, S.; Niemeyer, M.; Sattler, T.; and Geiger, A. 2022. MonoSDF: Exploring Monocular Geometric Cues for Neural Implicit Surface Reconstruction. In *NeurIPS*.

Yuan, W.; Gu, X.; Li, H.; Dong, Z.; and Zhu, S. 2023. Monocular Scene Reconstruction with 3D SDF Transformers. In *The Eleventh International Conference on Learning Representations, ICLR 2023, Kigali, Rwanda, May 1-5, 2023*. OpenReview.net.

Zhu, Z.; Peng, S.; Larsson, V.; Xu, W.; Bao, H.; Cui, Z.; Oswald, M. R.; and Pollefeys, M. 2022. NICE-SLAM: Neural Implicit Scalable Encoding for SLAM. In *IEEE/CVF Conference on Computer Vision and Pattern Recognition, CVPR 2022, New Orleans, LA, USA, June 18-24, 2022*, 12776–12786. IEEE.